

Optimization Study on Sliding Wear Characteristics and Heat-Treatment Conditions of Different Grades of Ferritic Ductile Cast Iron

V. Bramaramba¹ · S. Sen¹

Received: 1 December 2019 / Accepted: 9 March 2020 / Published online: 4 April 2020
© The Indian Institute of Metals - IIM 2020

Abstract The present work reports an experimental investigation on influence of microstructures on dry sliding wear performance of different grades of ferritic ductile iron. Ductile cast iron samples of ferritic grade have been subjected to different heat-treatment processes at different temperatures and times. Taguchi optimization technique (L_{16}) has been applied to evaluate the influence of different process variables (load, time, heat treatment, and grade) during ball-on-plate wear test. Meanwhile, analysis of variance (ANOVA) method was adopted to know the significance of aforesaid process variables. ANOVA results confirmed that the heat-treatment process has highest significance (54.76%) within all process variables. Among heat-treated specimens, austempered samples have outstanding wear resistance while the DMS samples have lower wear resistance. In addition, overall utility values have been evaluated by using individual utility values of weight loss and hardness. An obtained overall utility value gives the optimum combination for achieving higher wear resistance and hardness. Additionally, morphology of wear surfaces was examined in scanning electron microscope and the micrographs confirm the existence of inferior surface in terms of abrasive wear, adhesive wear, particle pullout and delaminated sheets on wear track. Enrichment of oxygen element has been observed on the worn path through energy-dispersive X-ray spectroscopy. X-ray diffraction analysis confirms the existence of different compounds like iron and silicon oxides on the wear track surface which may improve its hardness.

Keywords Ductile cast iron · Heat treatment · Wear · Optimization · ANOVA

1 Introduction

Ductile cast iron (DCI) is part of the cast iron series, also known as spherulitic iron or spheroidal graphite iron (SGI). It is a natural composite material. The name spheroidal graphite iron is derived from the spherical nature of graphite and can be used as a crack inhibitor to give material's excellent strength and toughness. DCI's are mainly classified based on the nature of their matrix phase like ferrite, pearlite, ferrite–pearlitic, martensite and austenite. Among them, ferritic ductile iron (FDI) has higher toughness and pearlitic ductile iron (PDI) has good wear resistance, moderate ductility, higher strength and impact resistance. Austempered ductile iron (ADI) is almost twice as strong as PDI and also retains high elongation and toughness [1–4].

In the present scenario, wear-resistant applications are enhancing their demand in various fields such as the automobile industry, defense field, construction, and railroad components. Generally, most of the components from the above fields are made from ductile iron (DI) family due to its special properties like higher strength, moderate ductility, and higher toughness and castability nature. However, components used in these fields are subjected to abrasive wear, erosive wear, adhesive wear, and fatigue wear. So, it is required to know the detailed wear behavior of the DI material to eliminate the failure of the aforesaid components. Zimba et al. [5] have investigated the abrasive wear behavior of ADI and found that wear resistance of ADI is more superior to its parent ductile material. They

✉ V. Bramaramba
vbrahmi@gmail.com

¹ Department of Metallurgical and Materials Engineering, NIT Rourkela, Rourkela 769008, India

also observed the surface transformation of retained austenite to martensite during abrasion wear which increases the surface hardness of [6] and [7]. They also investigated the abrasive and adhesive wear behavior of ADI material in a dry or lubricating sliding condition of rolling contact fatigue resistance of DCI and found that partially chilled as-cast DCI has highest rolling contact fatigue resistance than ADI. Zhang et al. [8] have conducted the rolling–sliding wear tests on dual-phase ADI material and reported that delamination is the main wear mechanism that is formed due to the subsurface deformation. Wear resistance of this dual-phase ADI material increases by the increase in matrix hardness. They also explored that the mechanical properties like tensile and yield strength increases with the increase in austenitizing temperature. Based on the results, the authors suggested that the 810 °C of austenitized temperature is suitable for achieving good wear resistance and enhanced mechanical properties for ADI material.

Zhang et al. [9] have studied the wear and friction properties of ADI with three different strength grades and found that delamination is the main deformation mechanism which decreases with an increase in matrix hardness. They also found that ADI (at 340 °C) is a suitable alternative to present rail track wheels because of its good wear performance, excellent mechanical properties, and reasonable friction properties. Islam et al. [10] have examined the tribological behavior of DCI samples under two heat-treatment processes, namely quenching & tempering and the austempering process by using pin-on-disk wear tests and observed that oxidative wear is the primary wear mechanism. They also concluded that quenching & tempering and austempering processes have nearly the same hardness but ADI has shown more durability than quenched & tempered ductile iron which is more prominent at higher loads and longer sliding distances. Sahin and Durak [11] have investigated the abrasive wear resistance of ADI materials at different austempering times using a pin-on-disk wear machine and explored the significance of process variables on abrasive wear resistance using analysis of variance (ANOVA) method. Among selected variables, sliding distance has the highest influence on abrasive wear at both austempering times (60 & 180 min). However, ADI of having 180 min of austempering time shows the better abrasive wear resistance than ADI of having 60 min of austempering time. Finally, they concluded that abrasive wear resistance increases with increasing austempering time in all materials. Yang and Putatunda [12] have examined the abrasive wear resistance of DI material using a two-step austempering process and compared it with the conventional austempering process. The authors observed that the two-step austempering process exhibits better abrasive wear resistance than the conventional

austempering process due to its improvement in microstructural parameters. Besides, material properties (yield strength) also have some influence on wear resistance of ADI.

Thus, from the above literature, it has been observed that a lot of research work has already been done on the wear behavior of DCI with different heat-treatment process. Many researchers have studied the influence of austempering time and temperature on wear behavior. Only a few authors have studied the influence of wear parameters (load, speed, and sliding distance) on wear behavior. So far no effort has been made on the comparison of wear resistance of different grades of ductile iron undergoing different heat-treatment processes. So the present study focuses on the wear behavior of different grades of ferritic ductile cast iron material subjected to different heat-treatment processes. Taguchi optimization technique has also been implemented to know the influence of different parameters (load, time, grade, and heat treatment) on the wear behavior of ductile iron material.

2 Experimentation

2.1 Materials

DCI test specimens of Y-blocks were cast with required composition mentioned in L & T, kansbahal, India. In the present investigation, ferritic ductile iron was taken as the initial material. The addition of silicon will develop and strengthen the ferrite in the DCI material [13]. The compositions of different grades of DCIs are mentioned in Table 1. The carbon equivalent for DCI specimens is useful for determining the final grain structure. Rectangular-shaped specimens were cut from the blocks with dimensions of 12 mm X 8 mm X 5 mm size to perform ball-on-plate wear test.

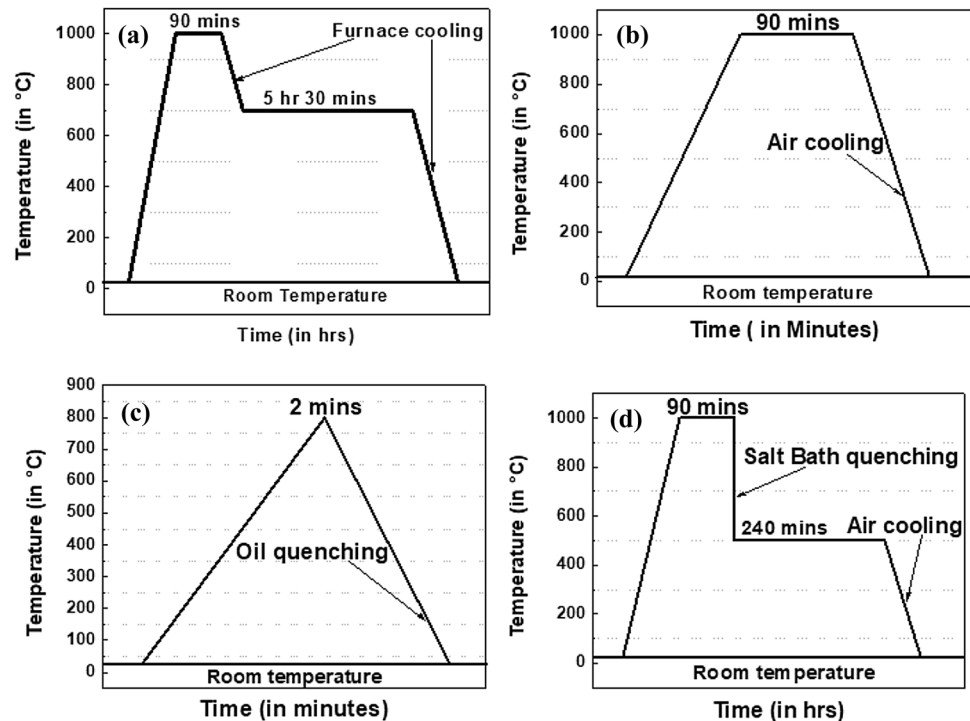
$$CE = \%C + 0.33(\%Si) + 0.33(\%P) - 0.027(\%Mn) + 0.4(\%S) \quad (1)$$

2.2 Heat Treatment

DCI specimens of four different grades (SG1, SG3, SG6, and SG7) were subjected to four different heat-treatment processes, viz., annealing, normalizing, austempering and dual matrix structure (DMS). The compositions of different grades of DCIs are mentioned in Table 1. The heat treatments were conducted by using OKAY raising hearth furnace (Max. Temp. 1700 °C) for austenitizing process and a pit furnace (Max. Temp. 2000 °C) was used for the austempering process. The four heat-treatment schedules

Table 1 Compositions of different grades of ductile iron

Alloy	%C	%Si	%Mn	%S	%P	%Cr	%Ni	%Mo	%Cu	%Mg	%Ce	%CE
SG-1	3.45	2.07	0.15	0.008	0.024	0.02	0.15	0.001	0.007	0.043	0.004	4.140
SG-3	3.59	2.01	0.17	0.009	0.023	0.01	0.45	0.001	0.007	0.026	0.006	4.259
SG-6	3.48	1.93	0.19	0.008	0.019	0.03	0.49	0.001	0.01	0.044	0.009	4.121
SG-7	3.63	2.19	0.25	0.008	0.033	0.03	0.09	0.001	0.014	0.042	0.0007	4.360

Fig. 1 Different heat-treatment processes; **a** annealing, **b** normalizing, **c** DMS, **d** austempering

are illustrated in Fig. 1. Here, all the samples were heat-treated at single-phase (austenite γ) region at 1000 °C and held there up to 90 min except for the DMS process. In the DMS process, samples were heated up to 800 °C with 2 min holding time. From Fig. 1, it was observed that the cooling medium and the holding time for the cooling process were different for the four heat-treatment processes. In the annealing process, samples were cooled in two stages. In the first stage, samples were furnace cooled up to eutectoid temperature (723 °C) and held there for 5 h 30 min to stabilize the ferrite and suppress the pearlite formation [14]. In the second stage, they were furnace cooled up to room temperature. Air cooling was done for normalized heat treatment. During the DMS heat-treatment process, samples were quenched in the mineral oil which acted as a cooling medium. In the austempering process, 50% KNO_3 + 50% NaNO_3 was used as the salt bath cooling medium where samples were cooled up to 500 °C and held there for 240 min. After that, samples were cooled in the air up to room temperature.

2.3 Wear Test (Ball-on-Plate)

Dry sliding wear tests were performed on heat-treated DCI samples using a DUCOM TR208-M1 ball-on-plate type tribometer equipped with a Rockwell barrel diamond indenter of 120° angle shown in Fig. 2. The diamond indenter was slid uni-directionally on the fixed samples to perform the wear test at room temperature (~ 27 °C). Samples were tested at four different loads (40 N, 80 N, 120 N & 160 N) and times (15 min, 30 min, 45 min & 60 min). After sample preparation, the entire sample's weight were taken before and after wear test with the help of digital weight balance of least count 0.1 mg (Make: Sartonic, Model: BSA2245-CW, Made: INDIA) for calculating the weight loss.

2.4 Experimental Design

Tribological investigation was carried out for all the heat-treated samples at different loads and times by using the

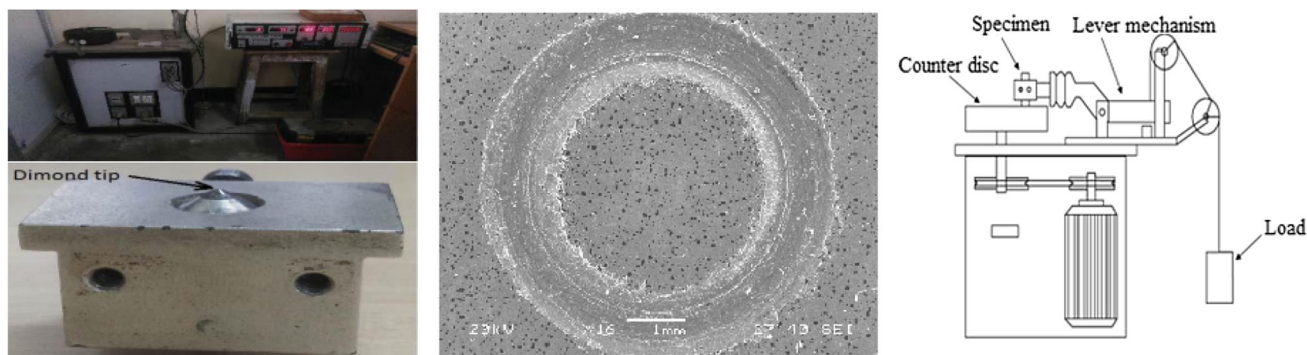


Fig. 2 Ball-on-plate wear test

ball-on-plate tribometer with a diamond indenter to know the effects of heat treatment on wear resistance of the different grades of DCIs. The code and levels of control parameters are shown in Table 2. The experimental plan consisted of four different input parameters, namely load, time, grade, and heat-treatment process with four different levels. So based on this, a standard Taguchi experimental plan with notation L_{16} (4 Factors and 4 Levels) was chosen as shown in Table 3.

2.5 Hardness Test

The four different types of heat-treated samples with different grades were subjected to hardness test before performing wear test. Hardness was done on Vickers hardness testing machine (Make: LECO & Model: LM248AT & MADE: Michigan, USA) by applying 100gf force, and dwell time was 10 s for all the samples. Nearly, 10 indentations were made for each sample and the average of those values was considered as hardness for particular sample.

2.6 X-ray Diffraction Analysis

X-ray diffraction analysis was carried out for the heat-treated samples after wear test to find out that if any precipitations or compounds might be formed on the wear surface. XRD measurements were conducted on a RIGAKU ULTIMA IV diffractometer with Cu K_α radiation

source. Experiments were performed with a two theta range of 40° – 90° , scan rate of $10^\circ/\text{min}$ and step size of 0.02° . The results were analyzed by using X'Pert Highscore software.

2.7 Microstructure Examination (Optical Microscopy and Scanning Electron Microscope)

The initial preparation of the samples was needed to observe the microstructure of the material. Rectangular samples were mounted and polished with 80 grid emery paper initially and then polished with fine emery papers (1/0, 2/0, 3/0, and 4/0) for a fine finish. After that, cloth polish along with alumina was done to remove the scratches on the surface of the sample for a mirror finish. Ultra-sonication was done for the polished samples with acetone before and after wear test to remove foreign material on the surface. Then, the microstructures of DCI samples were examined using an optical microscope. Pre-etched samples were examined for nodularity and nodule percentage. All the heat-treated samples were etched with 2% nital, and then, phases were studied under optical microscopy. Scanning electron microscope (SEM) was used to study the wear morphology of the worn surfaces of the wear track, and EDS analysis was also carried out for those worn surfaces to find out the different elements present in the material.

Table 2 Notations of selected parametric values and their ranges

Parameter	Symbol	Level 1	Level 2	Level 3	Level 4
Load (N)	A	40	80	120	160
Time (min)	B	15	30	45	60
Grade	C	SG 1	SG 3	SG 6	SG 7
Heat treatment	D	DMS	Annealed	Austempering	Normalizing

Table 3 Experimental Design of L_{16}

S. No.	Load (N) A	Time (min) B	Grade C	Heat treatment D	Weight difference (mg)	Average hardness (HV)
1	40	15	SG 1	DMS	0.6	259.4
2	40	30	SG 3	Annealed	0.4	304.7
3	40	45	SG 6	Austempering	0.1	414.3
4	40	60	SG 7	Normalizing	0.3	408.9
5	80	15	SG 3	Austempering	0.2	487.2
6	80	30	SG 1	Normalizing	0.3	386.3
7	80	45	SG 7	DMS	2.5	237.6
8	80	60	SG 6	Annealed	0.5	310.7
9	120	15	SG 6	Normalizing	0.2	415.4
10	120	30	SG 7	Austempering	0.3	479.4
11	120	45	SG 1	Annealed	2.6	346.6
12	120	60	SG 3	DMS	9.5	236.2
13	160	15	SG 7	Annealed	1.1	308.8
14	160	30	SG 6	DMS	5.0	285.9
15	160	45	SG 3	Normalizing	1.3	366.6
16	160	60	SG 1	Austempering	0.5	399.9

3 Taguchi Optimization Technique

The Taguchi optimization technique is a powerful statistical tool that allows the optimization process with the minimum number of experiments. In the Taguchi method, the experimental results are converted into a signal-to-noise ratio (S/N) or means. With the help of the S/N ratio values, the Taguchi method will estimate the quality characteristics that deviate from the desired values. Generally, S/N ratio values are analyzed based on three quality characteristics, which are the-nominal-the-better, the lower-the-better and the-higher-the-better. Depending on the required qualities of the output parameters, the related characteristic will be chosen. In the present investigation, weight loss should be minimized during wear test which specifies the wear resistance of the material. So, the lower-the-better notation was taken for calculating S/N ratio values. The S/N ratios for each level of test parameters were calculated based on the S/N analysis using MINITAB software. In addition, a statistical variance analysis (ANOVA) was performed to know which test parameters were statistically significant. Here, utility theory was also adopted for obtaining the optimal parametric value for a multi-objective function which consisted of different input parameters.

Utility maximization can be defined as the effectiveness of a product or process concerning the desired level of customer. The performance evaluation of each mechanical process depends on the number of output characteristics.

Therefore, comprehensive measures are needed to measure overall performance, taking into account all quality characteristics. Utility theory assumes that every decision is made based on the principle of maximization.

According to [15] and [16], the utility theory states that X_i is the measure of effectiveness of an attribute.

Here, i and n are quality characteristics and attributes evaluating the outcome space, then the joint utility function can be expressed as:

$$U(X_1, X_2, \dots, X_n) = f(U_1(X_1), U_2(X_2), \dots, U_n(X_n)) \tag{2}$$

Here, $U_i(X_i)$ is the utility of the i th attribute. The overall utility function is the sum of individual utilities if the attributes are independent, and is given as follows:

$$U(X_1, X_2, \dots, X_n) = \sum_{i=1}^n U_i(X_i). \tag{3}$$

The overall utility function after assigning weights to the attributes can be expressed as:

$$U(X_1, X_2, \dots, X_n) = \sum_{i=1}^n W_i \cdot U_i(X_i). \tag{4}$$

The preference number can be expressed on a logarithmic scale as follows:

$$P_i = A \times \log\left(\frac{X_i}{X_i^1}\right) \tag{5}$$

Here, X_i is the value of any quality characteristic or attribute i , X_i^1 is just acceptable value of quality

characteristic or attribute i and A is a constant. The value A can be found by the condition that if $X_i = X^*$ (where X^* is the optimal or best value), then $P_i = 9$. Therefore,

$$A = \frac{9}{\log \frac{X_i^*}{X_i}} \quad (6)$$

The overall utility can be expressed as follows:

$$U = \sum_{i=1}^n W_i P_i. \quad (7)$$

4 Results and Discussion

4.1 Microstructural Analysis

Figure 3 shows the pre-etching microstructures of DCI material subjected to four different heat-treatment processes. It shows that the austempered and normalized specimens have higher no. of nodules per unit area than those of annealed and DMS heat-treated specimens. The increased nodule count in austempered and normalized specimens is due to its faster rate of cooling. The high rate of cooling restricts the diffusion of carbon atoms from austenite into the parent graphite nodules resulting in increased nodule count as well as precipitation of secondary graphite particles.

Table 4 shows the nodule count of different heat-treatment processes for different grades. It is observed that the austempering process has a higher nodule count than other heat-treatment processes for all four different grades due to its higher cooling rate. SG3 grade has very less nodule count than SG1, SG6, and SG7 grades for all heat-treatment processes. The increase in magnesium content will

increase the nodularity of the DCI [17]. The lesser magnesium content of SG3 grade (see Table 1) may be the reason behind its least nodule count than the other three grades.

Microstructures obtained by different heat-treatment processes are illustrated in Fig. 4. As-cast samples consist of the fully ferritic matrix because of the higher amount of Si and Cr which promotes ferrite formation and suppresses the initiation of pearlite in the matrix [18]. This ferritic matrix has converted into different structures during different heat-treatment processes. The two-stage annealing process comprises a slow cooling rate resulting in the slower transformation of the parent matrix from the austenite stage, consequently achieving a fully ferritic matrix which is shown in Fig. 4c.

The normalizing heat treatment results in a pearlitic–ferritic matrix due to an increased rate of cooling as compared to an annealing process as shown in Fig. 4b. A higher transformation temperature leads to the lower driving force resulting in less growth rate of pearlite above the diffusion speed giving rise to large pearlite spacing, whereas lower temperature results in finer spacing [19]. The austempering process involves quenching of the sample in salt bath solution (50% KNO_3 + 50% NaNO_3) which is maintained at 500 °C and holding there for 240 min results in a coarse upper bainitic matrix with graphite nodules embedded into it as shown in Fig. 4a. Austempering involves a two-step reaction process consisting of transformation of primary austenite into acicular ferrite and carbon-enriched austenite in first stage reaction, and the second stage reaction comprises a decomposition of carbon-enriched austenite in ferrite-carbide aggregate depending on the temperature and time. The high

Fig. 3 Nodules of heat-treated samples; **a** DMS, **b** austempered, **c** annealed, **d** normalized

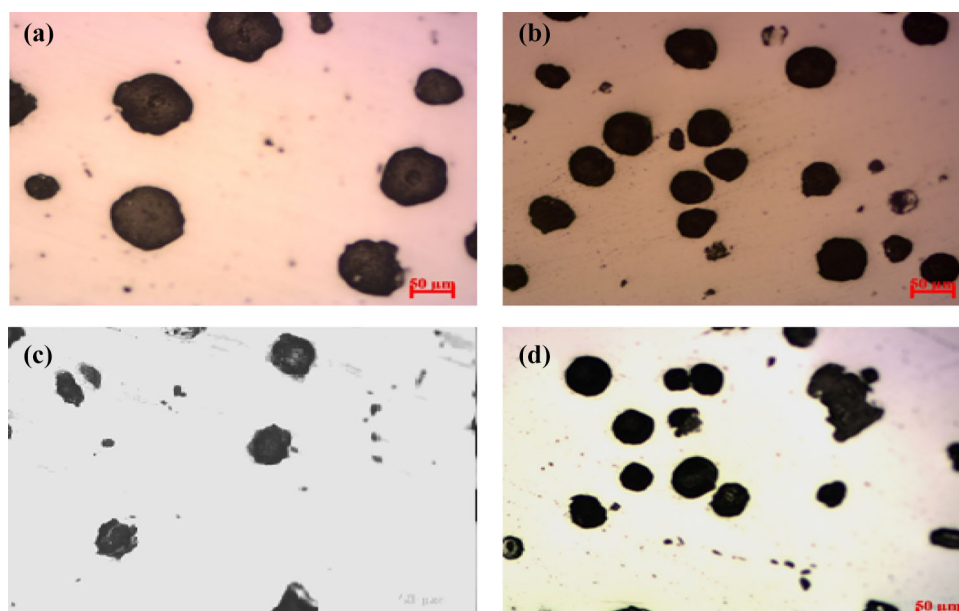
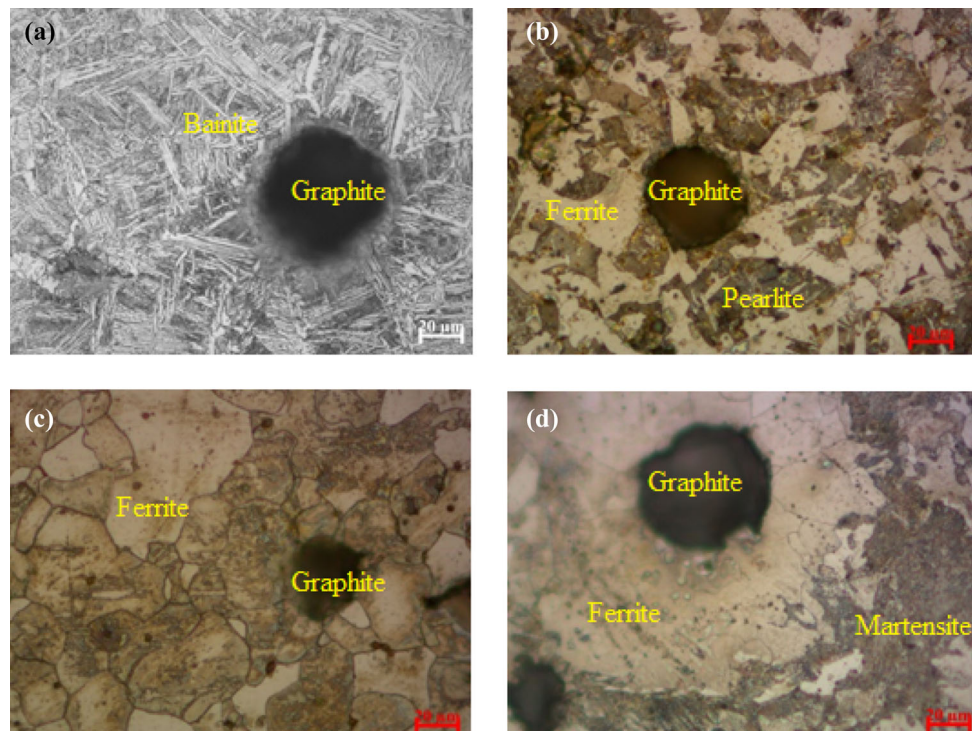


Table 4 Nodule count of the different heat-treatment process

	SG 1	SG 3	SG 6	SG 7
AUS	33	18	38	25
DMS	26	11	33	20
NORM	30	16	35	24
ANN	30	15	36	22

austenitizing temperature and longer austenitizing time result in increased stable austenite and less ferrite formation and also it coarsens the ferrite phase [20] and [21]. The austempered specimens are found to be free from carbide precipitation and martensite formation due to the higher austenitizing temperature and time (i.e., 500 °C and 240 min) which results in a complete austenitization process. In the intercritical austenitization, i.e., DMS heat-treatment process, the sample is quenched in mineral oil and cooled up to room temperature [22–25]. This process transforms the as-cast ferritic matrix into a combined ferrite and martensite matrix with graphite nodules surrounded by ferrite which is observed in Fig. 4d. Intercritical heat treatment commences with partial austenitization that depends on the alloy composition and temperature. The partial austenite transforms into martensite upon quenching in oil results in a final matrix consisting of graphite nodules embedded in ferrite + martensite.

Fig. 4 Microstructures of different heat-treated samples; **a** austempered (coarse upper bainitic), **b** normalized (pearlitic/ferritic), **c** annealed, and **d** DMS (ferrite + martensite)



4.2 Taguchi Optimization and ANOVA

The main effect plots between weight loss and different parameters are shown in Fig. 5. The direct effect (main) of load on weight loss of the ductile iron samples is shown in Fig. 5a. It is noticed that the weight loss increases with the increase in load. With an increase in load, the wear track width increases, which enhances the weight loss of the material. The direct effect (main) of time on weight loss of the ductile iron samples are presented in Fig. 5b. From this figure, it is observed that with increasing time, weight loss exhibits an increasing trend. This can be explained by the fact that with increasing time, the sliding distance covered by the diamond pointed tool on the workpiece also increases. Hence, weight loss increases with increasing time, irrespective of load, heat-treatment process and grades. The direct effect (main) of grade selection on weight loss of ductile iron samples are illustrated in Fig. 5c. Based on this result, it is found that, SG1, SG6 and SG7 grades have significantly less weight loss than the SG3 grade. Less magnesium content in SG3 grade yields less nodule count; by this it is prone to more weight loss than other grades. So we can conclude that SG3 grade has the lowest wear resistance than the other grades. The direct effect (main) of the heat-treatment process on weight loss of ductile iron samples is presented in Fig. 5d. It is shown that the weight loss is lower for the austempering heat-treatment process followed by normalizing, annealing, and DMS, respectively. That means the austempering process

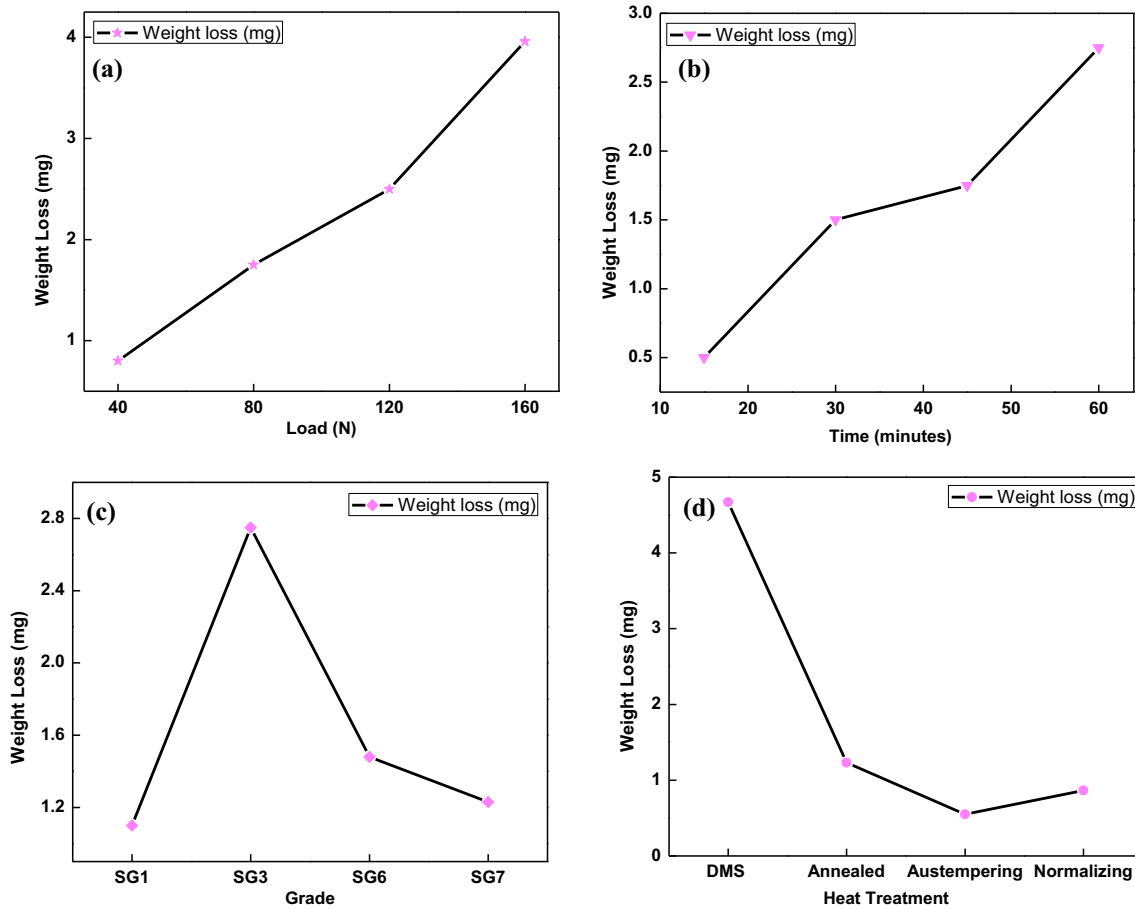


Fig. 5 Main effect plots of **a** load, **b** time, **c** grade selection and **d** heat-treatment process on weight loss

has higher wear resistance than the other heat-treatment processes. It is due to its bainite structure formation during the heat-treatment process. Normalizing heat treatment also has better wear resistance compared to annealing and DMS processes, due to the presence of pearlite in its microstructure.

The percentage contribution of each input parameter on the output responses has been calculated by performing ANOVA analysis using MINITAB software. Table 5 shows the ANOVA analysis by which we can find out the most significant parameter which influences the output response. From ANOVA analysis, it is found that heat treatment (P value of $0.036 < 0.05$) has the most influential contribution than other parameters for the weight loss during wear test of DCI samples. Heat treatment is the most significant parameter with a percentage contribution of 54.76% followed by load (26.52%) and time (7.45%). Among selected parameters, grade selection has the lowest influence (6.51%) on weight loss during wear test.

Individual utility of weight loss and hardness has been calculated by using Eq. 4 and overall utility has been measured by using Eq. 6 and those are tabulated in

Table 6. Based on overall utility values, means and S/N ratios are plotted in Figs. 6 and 7. From these plots, it is observed that heat treatment has more influence compared to other parameters and austempered samples have highest utility values. Overall utility value helps to predict the optimum combination which has good wear resistance and hardness. And, the optimum parametric setting is $A_2B_1C_2D_3$ (contains 8.314 overall utility value); means 80 N of load, 15 min of time, grade 3 composition and austempering heat treatment offer good wear resistance and hardness within the considered combinations of parameters (sixteen).

However, both means and S/N ratios values offer the optimal overall utility value at a particular combination of parametric setting, i.e., $A_1B_1C_3D_3$ (as shown in Figs. 6, 7). Here, A, B, C, D represents the input parameter's load, time, grade and heat-treatment processes, respectively, whereas 1, 2, 3, 4 represents their levels which can be observed from Table 2. So, A_1 represents 40 N load, B_1 represents 15 min time, C_3 represents SG6 grade and D_3 represents austempering process. That means wear test conducted for SG6 grade of DCI material subjected to

Table 5 Analysis of variance for weight loss using adjusted SS test

Source	DF	SS	MS	<i>F</i>	<i>P</i>	Contribution (%)
A	3	23.451	7.817	5.58	0.096	26.52
B	3	6.591	2.197	1.57	0.36	7.45
C	3	5.763	1.921	1.37	0.401	6.51
D	3	48.431	16.144	11.52	0.037*	54.76
Error	3	4.204	1.401			4.75
Total	15	88.44				100

*Significant parameters at 5% significance level

Table 6 Utility value of individual response

Sl. No.	Individual utility values		Overall utility index	Ranking
	<i>U</i> weight loss	<i>U</i> hardness		
1	5.458774	1.164661	3.311718	13
2	6.260095	3.166505	4.7133	8
3	8.999829	6.984339	7.992084	2
4	6.828641	6.821995	6.825318	5
5	7.629962	9.000000	8.314981	1
6	6.828641	6.115204	6.471923	6
7	2.638363	0.073461	1.355912	15
8	5.819096	3.40889	4.613993	10
9	7.629962	7.018799	7.32438	4
10	6.828641	8.798719	7.81368	3
11	2.560851	4.768933	3.664892	12
12	0	0	0	16
13	4.260867	3.333651	3.797259	11
14	1.268496	2.37599	1.822243	14
15	3.930718	5.46537	4.698044	9
16	5.819096	6.546879	6.182988	7

austempering heat-treatment process at 40 N load with 15 min time produces optimum wear resistance and hardness. This parametric setting value has higher hardness and minimum weight loss than other combination of parameters in 4 factors and 4 levels (means 4^4 or 256 combinations).

4.3 Study of Wear Track Width

The variation of hardness and wear track width with respect to different heat-treatment processes (austempering, normalizing, annealing and DMS) is shown in Fig. 8. Here, the hardness has been taken as average of the output values obtained from L_{16} Taguchi method. By using stereo microscope, width of the wear track is measured in different places on the wear track of all grades with the help of Axio-Vision Release 4.8.2 software and average value is

calculated. It is noticed that austempered samples have higher hardness and lower wear track width followed by normalizing, annealing and DMS processes. The bainitic structure of austempered samples yield higher hardness and lower wear track width than the other heat-treatment processes. It is known that DMS heat-treated samples consist of ferrite + martensite structure, but because their lower volume fraction of martensite, it has least hardness and higher wear track width. So, austempered samples have higher wear resistance and DMS samples have lower wear resistance among the other heat-treatment processes.

4.4 Morphological Study of Wear Tracks

Figure 9 shows the wear track images for different heat-treated samples which have been used to study the wear mechanisms during wear test. However, the wear track

Fig. 6 Main affects plots for means considering overall utility

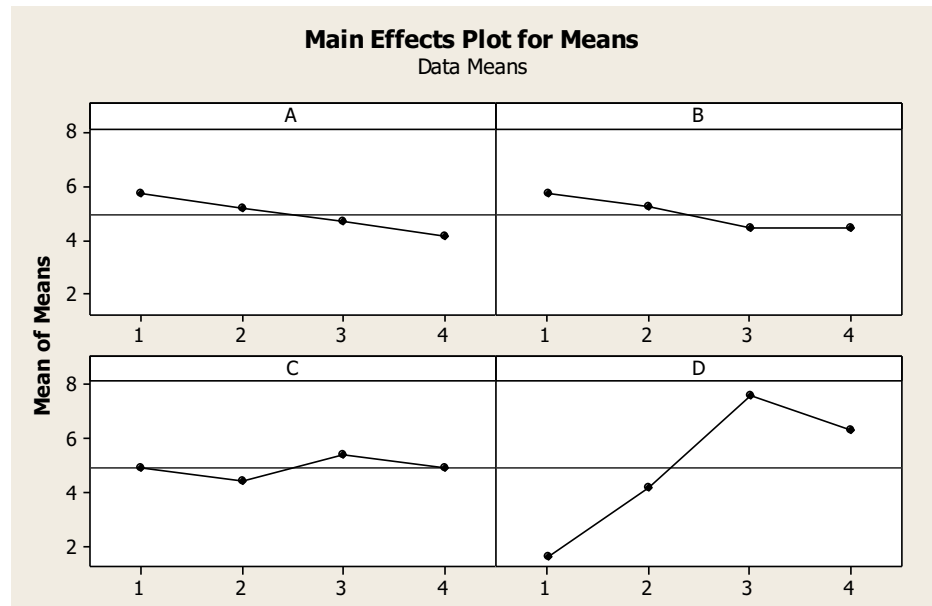
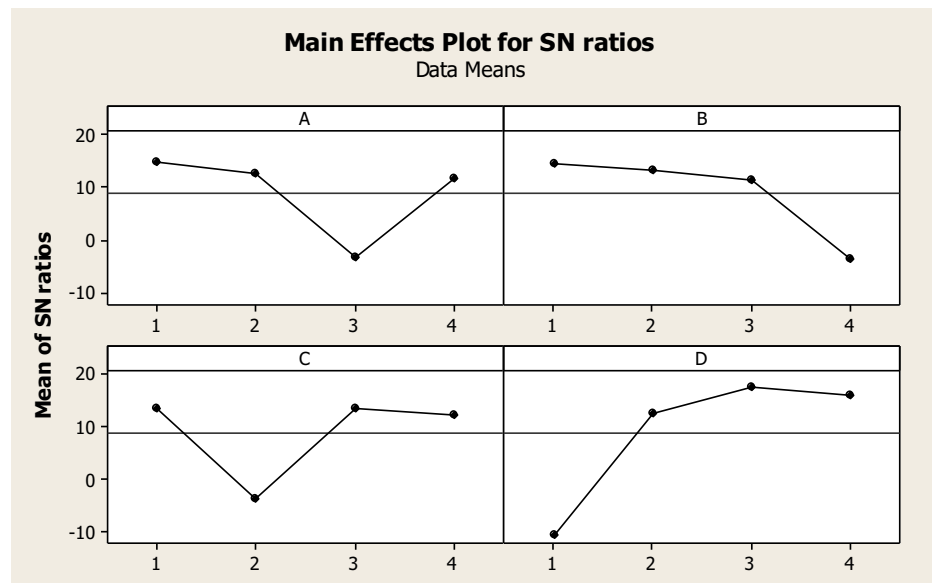


Fig. 7 Main affects plots for S/N ratios considering overall utility



images consists of inferior surface due to the existence of micro-cracks, delaminated sheets, oxide layers and some surface damages created by abrasive and adhesive wear mechanisms. While performing wear operation, some stresses are generated within the base material. Whenever these induced stresses exceed the ultimate strength of the work material, then cracks are formed over the wear track. Particle pullout takes place due to the presence of hard particles residing over the wear track and these are pulled out from the track during wear test. Adhesive wear is observed over the wear track. Adhesive wear is formed due to the deformation of the softer material by harder tool tip during wear test. While doing test, softer part of the material is dragged away by the diamond tool and this adheres on the

other part of the surface which looks like plate like morphology over the wear track. In addition, abrasive wear is also noticed on the wear track and this one occurs due to the penetration of harder particles in the softer material. These hard particles acts as the third body in between the contact surfaces and changes the wear mechanism from two body to three body abrasion which results in raising of thin flat sheets, which later results in delamination of the wear track. But due to the tangential motion, these harder particles in the softer surface are removed by combined effects of 'micro-plowing,' 'micro-cutting' and 'micro-cracking' and forms line traces over the wear track.

Delamination wear mechanism is clearly observed in DMS process in addition to the abrasive wear, crack and

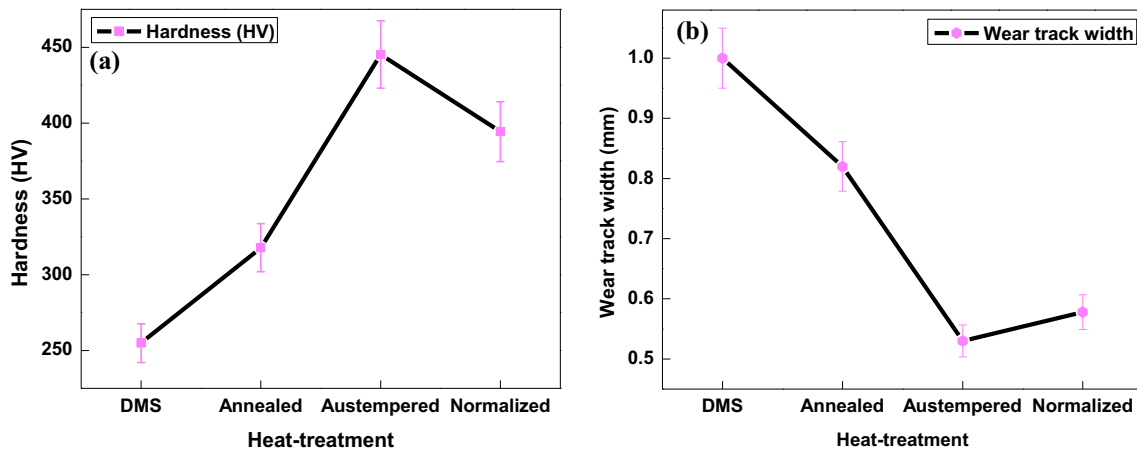


Fig. 8 Effect of heat treatment on a hardness and b width of the wear track

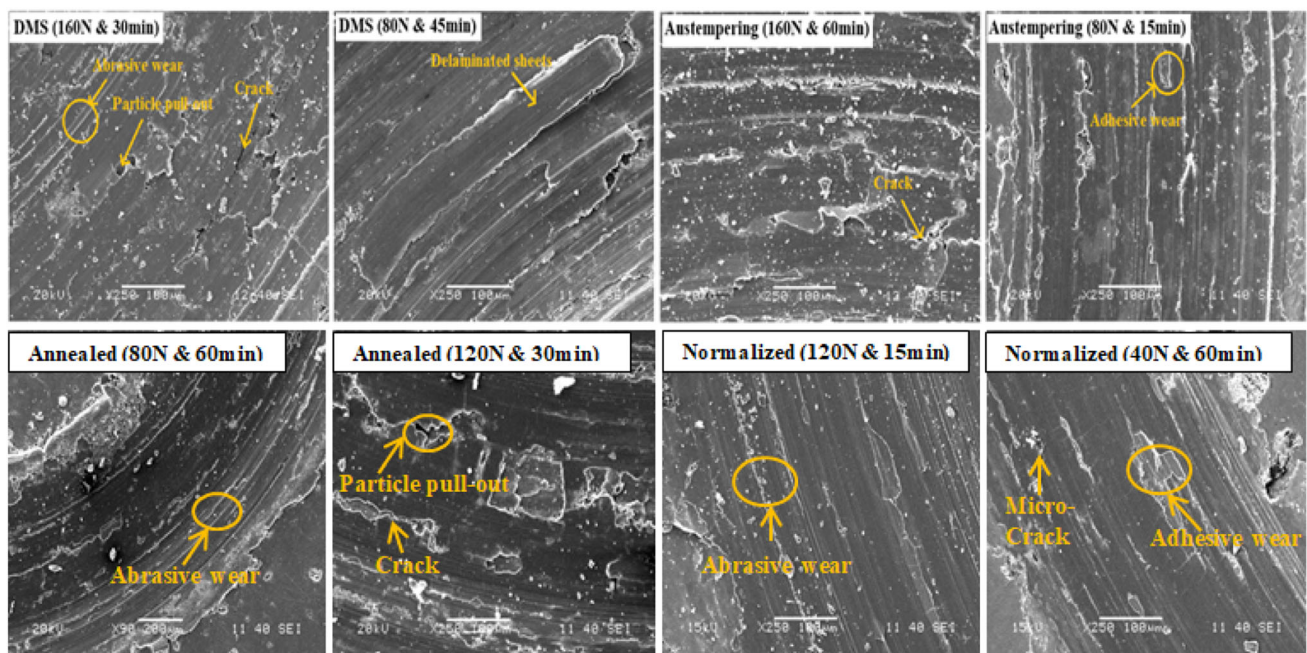


Fig. 9 Morphology of wear track images for different heat-treated samples

particle pullout mechanisms. Because of the lower wear resistance and lesser hardness of DMS heat-treated samples, it is easier to remove the wear surface as delaminated sheets. Annealed samples mainly consist of abrasive wear mechanism including particle pullouts and crack propagation failure. Austempering process involves in crack propagation and adhesive wear mechanisms during wear test. Austempered samples consist of only lesser number of wear failure mechanisms because of its higher wear resistance. In normalized samples, both adhesive and abrasive wear mechanisms are observed including micro-cracks formation.

4.5 EDS Analysis

The elemental distribution of as received material and wear zone of different heat-treated samples (grade 6) are represented in Figs. 10, 11, 12 and 13. EDS elemental spectra reveal the chemical composition of the work material before and after the wear test. The enrichment of oxygen element in the zone of wear track in comparison with the base metal is noticed for all the heat-treated samples as shown in Table 7. This happens mainly due to the high reactivity of iron in its composition. During wear test, higher temperatures are generated at the interaction zone (between diamond pin and work surface). At higher temperatures, the reactivity of iron and carbon is more than

Fig. 10 EDS of austempered sample (Grade 6) at **a** base material, **b** wear track

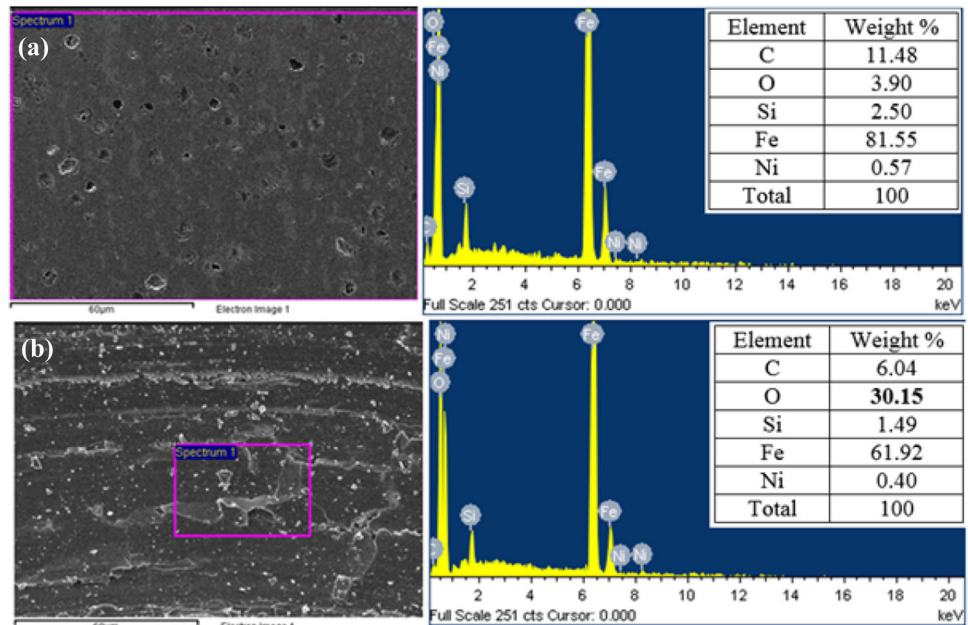
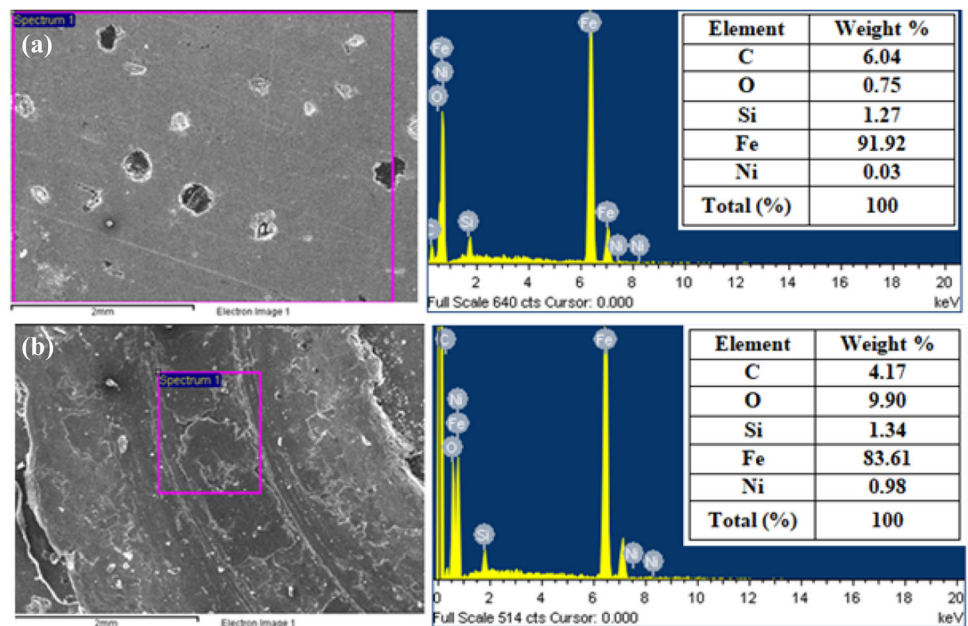


Fig. 11 EDS of annealed sample (Grade 6) at **a** base material, **b** wear track



that in normal condition. Because of this reason, during wear test, parent material reacts with the oxygen present in environment and forms oxides over the wear track. This enhanced oxygen percentage can be compensated by reducing the other elements (iron and carbon) in their composition which is clearly noticed from Figs. 10, 11, 12 and 13. Using line EDS method, the difference in elemental distribution along the wear path and base material can be clearly noticed. The line EDS of normalizing sample of grade 6 is shown in Fig. 14. From this it can be noticed that oxygen and iron percentages vary along the wear path.

At starting of the wear track, i.e., near to the base material, the percentage of the oxygen is less. Its value gradually increases along the wear zone, afterward again its value decreases at the end of the wear track. In contrast to the oxygen enrichment, there is a decrement in iron percentage, which is clearly observed along the wear track. Iron percentage is higher in base material, and its value decreases while moving toward the wear track and it again increases at the end of the wear track. So based on this, we can tell that the increased percentage of oxygen will be redacted from iron and other elements.

Fig. 12 EDS of normalized sample (Grade 6) at **a** base material, **b** wear track

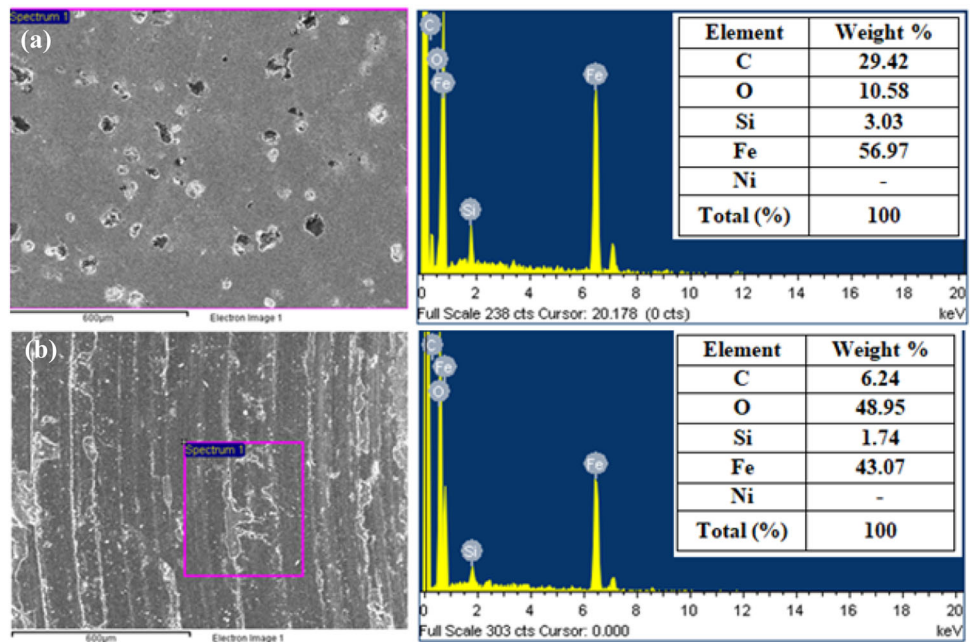
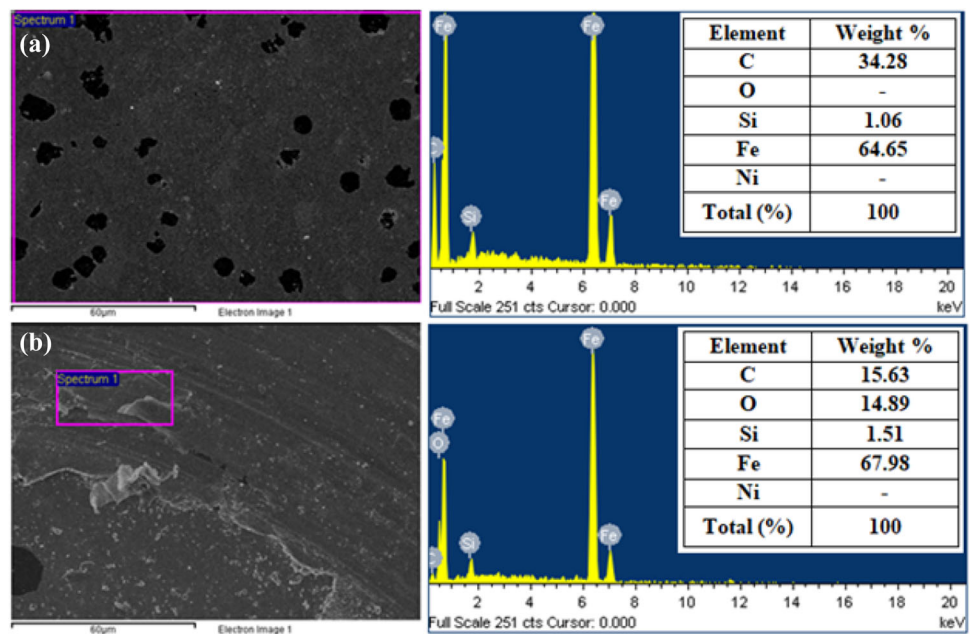


Fig. 13 EDS of DMS sample (Grade 6) at **a** base material, **b** wear track



4.6 XRD Analysis

Figure 15 shows the X-ray diffraction analysis by using I versus 2θ graphs for two different heat-treated samples. XRD experiments have been performed for both base material and wear track surface. The formation of bainite and austenite peaks are observed during austempering process [26] and [27]. Along with these, the formation of iron carbide (Fe_3C), iron oxides (such as Fe_2O_3 and Fe_3O_4), silicon dioxide (SiO_2) and silicon carbide (SiC) precipitates

are also clearly observed on the wear track surface of the austempered and normalized samples. This is due to the generation of heat during the wear test which enhances the reactivity of the base material with atmosphere. These precipitates will increase the hardness of the wear surface and resist the further weight loss during the wear test. So, the wear resistance for austempered and normalized samples is observed to be more than the other heat-treated samples.

Table 7 Elemental distribution of different heat-treated samples

Element	Weight (%)							
	Aus-SG 6		Nor-SG 6		An-SG 6		DMS-SG 6	
	Base	Wear path	Base	Wear path	Base	Wear path	Base	Wear path
C	11.48	6.04	29.42	6.24	6.04	4.17	27.04	15.63
O	3.90	30.15	10.58	48.95	0.75	9.90	2.12	14.89
Si	2.50	1.49	3.03	1.74	1.27	1.34	1.06	1.51
Fe	81.55	61.92	56.97	43.07	91.92	83.61	69.65	67.77
Ni	0.57	0.40	0.03	0.06	0.03	0.98	0.12	0.21
Total (%)	100	100	100	100	100	100	100	100

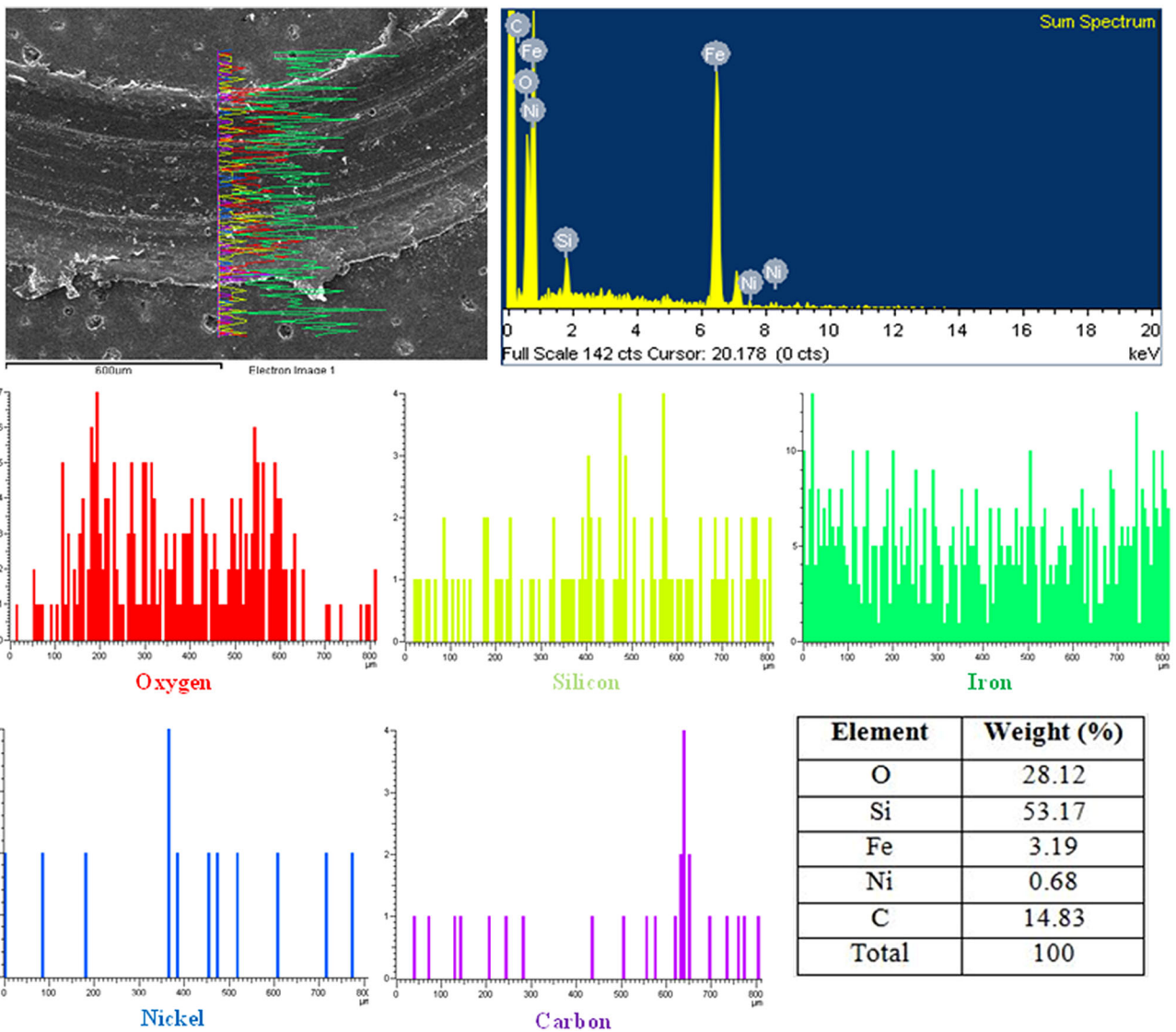
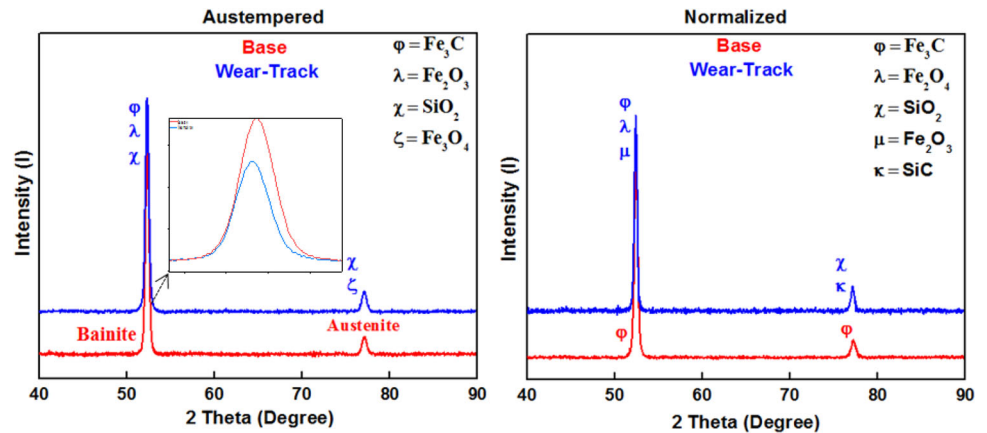


Fig. 14 EDS along the distance of normalized wear track (Grade 6)

Fig. 15 X-ray diffraction analysis of grade-6 austempered and normalized samples



5 Conclusions

In the present investigation, different grades of ferritic ductile iron (SG1, SG3, SG6 and SG7) were subjected to different heat-treatment processes (DMS, annealing, normalizing and austempering). Later, wear test was performed for these samples by using L16 Taguchi optimization technique. From above results the following conclusions can be drawn:

1. According to L_{16} Taguchi optimization technique, heat treatment is the most influential parameter followed by load, time and grade for wear behavior of the DCI material. From utility theory, it is obtained that $A_1B_1C_3D_3$ be the optimum parametric combination which satisfies the optimum wear resistance and hardness. So, SG6 grade of DCI material heat-treated with austempering process subjected to wear test at 40 N load and 15 min time yields the optimum wear resistance and hardness than the other combination of parameters.
2. Increase in load and time has increased the weight loss during wear test. Austempering process has maximum wear resistance compared to the other heat-treatment processes. SG3 grade has minimum wear resistance than the other grades of DCI material.
3. Morphology of wear track images has been studied by using SEM analysis. DMS samples are more prone to delamination wear mechanism than other heat-treated samples. Other mechanisms like abrasive wear, adhesive wear, micro-cracks and particle pullouts are also clearly observed on the wear surfaces of other heat-treatment processes.
4. The wear track width values have been correlated with hardness values for different heat-treatment processes. Austempering process yields higher hardness and lower wear track width. While the DMS has lower hardness and higher wear track widths because of its

lower wear resistance among other heat-treatment processes.

5. EDS analysis confirms oxygen enrichment over the wear track surfaces during wear test. The compounds like iron oxides and silicon oxides have been identified over the wear surface by XRD analysis.

References

1. Konečná R, Nicoletto G, Bubenko L, and Fintová S, *Eng Fract Mech* **108** (2013) 251.
2. Dommarco R C, Sousa M E, and Sikora J A, *Wear* **257** (2004) 1185.
3. Rashidi A M, and Moshrefi-Torbati M, *Mater Lett* **45** (2000) 203.
4. Zhou R, Jiang Y, Lu D, Zhou R, and Li Z, *Wear* **250** (2001) 529.
5. Zimba J, Simbi D J, and Navara E, *Cem Concr Compos* **25** (2003) 643.
6. Magalha L, and Seabra J, *Wear* **215** (1998) 237.
7. Dommarco R C, and Salvande J D, *Wear* **254** (2003) 230.
8. Zhang H, Wu Y, Li Q, and Hong X, *Wear* **406** (2018) 156.
9. Zhang N, Zhang J, Lu L, Zhang M, Zeng D, and Song Q, *Mater Des* **89** (2016) 815.
10. Islam M A, Haseeb A S M A, and Kurny A S W, *Wear* **188** (1995) 61.
11. Sahin Y, and Durak O, *Mater Des* **28** (2007) 1844.
12. Yang J, and Putatunda S K, *Mater Sci Eng A* **406** (2005) 217.
13. Mallia J, Grech M, and Smallman R E, *Mater Sci Technol* **14** (1998) 452.
14. Górný M, and Tyrála E, *J Mater Eng Perform* **22** (2013) 300.
15. Kumar P, Barua P B, and Gaidhar J L, *Qual Reliab Eng Int* **16** (2000) 475.
16. Walia R S, Shan H S, and Kumar P, *Mater Manuf Process* **21** (2006) 907.
17. Omran A M, Abdel-Jaber G T, and Ali M M, *Int J Eng Res Appl* **4** (2014) 90.
18. Gonzaga R A, and Carrasquilla J F, *J Mater Process Technol* **162** (2005) 293.
19. Bockus S, and Zaldarys G, *Mater Sci Medzg* **16** (2010) 307.
20. Putatunda S K, and Gadicherla P K, *Mater Sci Eng A* **268** (1999) 15.
21. Fordyce E P, and Allen C, *Wear* **135** (1990) 265.

22. Elsayed A H, Megahed M M, Sadek A A, and Abouelela K M, *Mater Des* **30** (2009) 1866.
23. Achary J, *J Mater Eng Perform* **9** (2000) 56.
24. Delia M, Alaalam M, and Grech M, *Journal of Materials Engineering and Performance* **7** (1998) 265.
25. Erfanian-Naziftoosi H R, Haghdadi N, and Kiani-Rashid A R, *J Mater Eng Perform* **21** (2012) 1785.
26. Talebi S H, Ghasemi-Nanesa H, Jahazi M, and Melkonyan H, *Metals* **7** (2017) 346.
27. Dong H Y, Wu K M, Wang X L, Hou T P, and Yan R, *Wear* **402** (2018) 21.

Publisher's Note Springer Nature remains neutral with regard to jurisdictional claims in published maps and institutional affiliations.